Mechanistic details of a protein–protein association pathway revealed by paramagnetic relaxation enhancement titration measurements

Nicolas L. Fawzi[1], Michaeleen Doucleff[1], Jeong-Yong Suh, and G. Marius Clore[2]

Laboratory of Chemical Physics, National Institute of Diabetes and Digestive and Kidney Diseases, National Institutes of Health, Bethesda, MD 20892-0520

Edited by Alan R. Fersht, Medical Research Council Centre for Protein Engineering, Cambridge, United Kingdom, and approved November 18, 2009 (received for review August 17, 2009)

Protein–protein association generally proceeds via the intermediary of a transient, lowly populated, encounter complex ensemble. The mechanism whereby the interacting molecules in this ensemble locate their final stereospecific structure is poorly understood. Further, a fundamental question is whether the encounter complex ensemble is an effectively homogeneous population of nonspecific complexes or whether it comprises a set of distinct structural and thermodynamic states. Here we use intermolecular paramagnetic relaxation enhancement (PRE), a technique that is exquisitely sensitive to lowly populated states in the fast exchange regime, to characterize the mechanistic details of the transient encounter complex interactions between the N-terminal domain of Enzyme I (EIN) and the histidine-containing phosphocarrier protein (HPr), two major bacterial signaling proteins. Experiments were conducted at an ionic strength of 150 mM NaCl to eliminate any spurious nonspecific associations not relevant under physiological conditions. By monitoring the dependence of the intermolecular transverse PRE (Γ_2) rates measured on ^{15}N-labeled EIN on the concentration of paramagnetically labeled HPr, two distinct types of encounter complex configurations along the association pathway are identified and dissected. The first class, which is in equilibrium with and sterically occluded by the specific complex, probably involves rigid body rotations and small translations near or at the active site. In contrast, the second class of encounter complex configurations can coexist with the specific complex to form a ternary complex ensemble, which may help EIN compete with other HPr binding partners in vivo by increasing the effective local concentration of HPr even when the active site of EIN is occupied.

enzyme I-histidine containing phosphocarrier protein complex | encounter complex | lowly populated states | NMR | phosphotransferase system

Specific protein–protein interactions underlie virtually every process in the cell. In general, specific protein–protein recognition proceeds via a two-step process (1–3): weak association via diffusion-controlled intermolecular collisions results in the formation of an ensemble of short-lived, encounter complexes located in multiple local free energy minima of a two-dimensional funnel-like energy landscape on the protein surface (4); subsequent rearrangement along the energy landscape, involving translations and rotations of the two partner proteins, permits the global free energy minimum to be located, resulting in the formation of a well-defined specific complex stabilized by a defined set of electrostatic and van der Waals interactions. From a functional perspective, encounter complex ensembles are thought to play a critical role in fine tuning reaction fluxes inside the cell (5), enhancing association on-rates by increasing the interaction cross-section and reducing the conformational search space on the path to the specific complex (6–11). Despite the importance of encounter complex ensembles in protein–protein association, little is known of their structures and configurations because their populations are low, their lifetimes are short, and they are difficult to trap, rendering them essentially invisible to conventional structural and biophysical methods. Recently, however, the application of NMR paramagnetic relaxation enhancement (PRE), a technique that is exquisitely sensitive to the presence of lowly populated states in the fast exchange regime (12, 13), has offered new insights into the physicochemical and structural nature of transient encounter complexes in protein–DNA (14) and protein–protein (15–20) association. The mechanism, however, whereby the interacting molecules in the encounter complex ensemble find their final stereospecific structure, remains poorly understood.

The underlying principle behind this application of the PRE is as follows (13, 14). The transverse PRE rate (Γ_2) is dependent on the sixth root of the distance between the unpaired electron of the paramagnetic center and the observed proton, and the Γ_2 rate at short distances is very large owing to the large magnetic moment of the unpaired electron (21). In the fast exchange regime, the observed Γ_2 rates are population weighted averages of the Γ_2 rates in the major and minor species, and hence the footprint of minor species can be observed in the PRE profiles of the major species, providing that distances between the paramagnetic label and protons of interest are shorter in the minor species than in the major one. This technique has also been used to determine the structure of a lowly populated state of a multidomain protein in which large interdomain motions accompany ligand binding (22), and to probe qualitatively the configurations sampled by unfolded and intrinsically disordered proteins (23–25).

In previous PRE work on several relatively weak protein–protein complexes (15), we showed that the encounter complex ensemble comprises a relatively diffuse cloud that correlates qualitatively with the electrostatic surface potentials of the partner proteins. The intermolecular PREs attributable to the encounter complex ensemble are significantly more sensitive to ionic strength than those arising from the specific complex, confirming a prominent role for electrostatic forces in stabilizing the encounter complex ensemble (26). A fundamental question arises as to whether the encounter complex ensemble represents a homogenous population of nonspecific complexes or a collection of distinct states.

To address this question, we carried out intermolecular PRE titration measurements using the complex between the N-terminal domain of Enzyme I (EIN) and the histidine phosphocarrier protein (HPr) as a model system. By monitoring the residue-specific intermolecular PRE rates observed on ^{15}N-labeled

Author contributions: N.L.F., J.-Y.S., and G.M.C. designed research; N.L.F., M.D., and J.-Y.S. performed research; N.L.F., M.D., J.-Y.S., and G.M.C. analyzed data; N.J.F., M.D., and G.M.C. wrote the paper.

The authors declare no conflict of interest.

This article is a PNAS Direct Submission.

[1]N.L.F. and M.D. contributed equally to this work.

[2]To whom correspondence should be addressed: E-mail: mariusc@mail.nih.gov.

This article contains supporting information online at www.pnas.org/cgi/content/full/0909370107/DCSupplemental.

EIN as a function of the concentration of paramagnetically labeled HPr, we are able to identify and dissect two distinct classes of encounter complexes within the energy landscape of protein–protein association and specific complex formation. The first class of encounter complexes is in equilibrium with and sterically occluded by the specific complex (i.e., it directly competes sterically with the specific complex). In contrast, the second class of encounter complexes can coexist with the specific complex to form a ternary complex ensemble. It is likely that these two classes of encounter complexes play different roles in accelerating phosphoryl transfer reaction fluxes between Enzyme I and HPr in vivo.

Results and Discussion

Concentration-Dependent Nonspecific PREs Indicate the Presence of Multiple Encounter Complex Configurations. In the first step of the bacterial phosphotransfer system (PTS), a signal transduction pathway in which sugar transport across the membrane is coupled to phosphotransfer via a series of bimolecular protein–protein complexes (27), phosphoryl transfer between EIN and HPr occurs upon formation of a specific interaction that properly aligns the active site histidines of the two proteins (28). This productive association of EIN and HPr has an equilibrium dissociation constant (K_D) in the micromolar range (26, 29). Exchange between the specific complex, nonspecific encounter complex configurations and the free (dissociated) state is fast on both the chemical shift (28) and PRE relaxation (15) time scales, allowing intermolecular PREs to report on transient encounter complex configurations along the EIN/HPr association pathway (15, 26).

HPr (at natural isotopic abundance) was labeled with a paramagnetic EDTA-Mn^{2+} moiety conjugated via a disulfide bond to surface cysteine mutations at the three sites used in previous studies (15, 26): E25C and E32C are located on opposite sides of the specific binding surface, whereas E5C is located on the opposite face of HPr (Fig. 1 insets). These three tags are located outside the specific interaction surface with EIN and, hence, do not interfere with the formation of the specific complex, and provide good coverage to probe both the specific complex and the encounter complex ensemble. Intermolecular ^1H_N-Γ_2 rates for the backbone amide protons of U-[^{2}H, ^{15}N]-labeled EIN (Fig. 1) in the presence of paramagnetically labeled HPr were measured as described previously (15), except that the experiments were carried out in the presence of 150 mM NaCl to eliminate potential spurious nonspecific interactions not relevant at physiological ionic strength.

Back-calculation of the expected intermolecular PREs from the structure of the specific EIN/HPr complex (15) (Fig. 1, black line) permits one to partition the experimental intermolecular PREs into two classes: (*i*) PREs that arise from only the specific complex (Fig. 1, black circles), which we refer to as "specific PREs"; and (*ii*) PREs arising from the encounter complex ensemble (Fig. 1, purple circles), which we refer to as "nonspecific PREs." The latter comprise residues that meet the following criteria in a sample consisting of 300 μM EIN and 450 μM HPr: (*i*) the ^{1}H-^{15}N cross-peak is well-resolved, (*ii*) the predicted specific ^1H_N-Γ_2 rate is <20 s^{-1} because both the predicted and experimental ^1H_N-Γ_2 rates become relatively imprecise at higher values, and (*iii*) the observed ^1H_N-Γ_2 rate is ≥ 8 s^{-1} above the intermolecular ^1H_N-Γ_2 rates back-calculated from the specific EIN/HPr complex. This last cutoff (8 s^{-1}) was chosen because it is twice the standard deviation (3.8 s^{-1}) of the difference between the observed and calculated ^1H_N-Γ_2 rates for PREs with an observed Γ_2 rate of <20 s^{-1} arising from the HPr-E25C probe (see below). Using the above criteria, nonspecific intermolecular PREs occur at residues 59-75, 111-117, and 160-167 for EIN/HPr-E5C, and residues 22-51, 56-74, 96-106, and 160-167 for EIN/HPr-E32C (Fig. 1, purple circles).

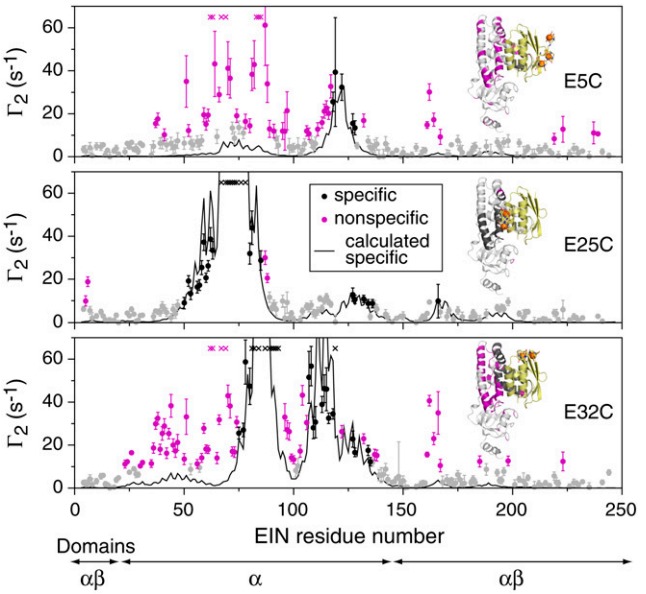

Fig. 1. Intermolecular ^1H_N-Γ_2 PRE profiles observed on U-[^{2}H, ^{15}N]-labeled EIN from a paramagnetic EDTA-Mn^{2+} moiety on HPr E5C (*Top*), E25C (*Middle*), or E32C (*Bottom*) at an ionic strength of 150 mM NaCl. The concentrations of EIN and HPr are 300 and 450 μM, respectively. Theoretical intermolecular PREs ($\Gamma_2^{calc,specific}$) back-calculated (15) from the coordinates of the specific EIN/HPr complex (28) are shown as black lines. Experimental intermolecular PREs are displayed as filled-in circles as follows. The nonspecific intermolecular PREs (i.e., PREs attributed to the encounter complex ensemble) are in purple and defined by the following criteria: $\Gamma_2^{obs} > (\Gamma_2^{calc,specific} + 8\ s^{-1})$ and $\Gamma_2^{calc,specific} < 20\ s^{-1}$ (because a large value of $\Gamma_2^{calc,specific}$ precludes the reliable identification of a superimposed nonspecific PRE). The specific intermolecular PREs (i.e., PREs attributed to the specific complex) are in black and defined by the criteria that both $\Gamma_2^{calc,specific}$ and $\Gamma_2^{obs} > 8\ s^{-1}$ (see *Methods*). The remaining intermolecular PREs are in gray. Crosses indicate residues with ^{1}H-^{15}N cross-peaks that are broadened beyond detection by PRE. (*Inset*) Specific (black) and nonspecific (purple) intermolecular PREs mapped onto the surface of EIN (gray ribbons) with HPr (yellow) in the specific configuration; the EDTA-Mn^{2+} label is represented by a three-conformer ensemble (15) with the Mn^{2+} atoms shown as orange spheres.

At an ionic strength of 150 mM, the intermolecular PREs generated by HPr-E25C are almost entirely accounted for by the specific EIN/HPr complex (except for PREs at residues 5, 6, 87, and 88) (Fig. 1 *Middle*). Although this may seem surprising, examination of the PRE profiles for the three probes indicates that the majority of residues exhibiting nonspecific PREs for the EIN/HPr-E5C and EIN/HPr-E32C complexes coincide with residues that display specific PREs for the EIN/HPr-E25C complex, thereby largely precluding the observation of nonspecific PREs for the EIN/HPr-E25C complex (because the observation of encounter complex PREs requires that a given paramagnetic label-EIN proton distance be much shorter in the encounter complex ensemble than in the specific complex). Thus, the PRE profile for the EIN/HPr-E25C complex not only provides an excellent reference for estimating the uncertainties in our measurements and fits, but also confirms the robustness of the PREs back-calculated from the structure of the specific EIN/HPr complex (Fig. 1 *Middle*).

Intermolecular PRE measurements on U-[^{2}H, ^{15}N]-labeled EIN were carried out at six different concentrations of paramagnetically labeled HPr (ranging from 60 to 450 μM), corresponding to HPr:EIN molar ratios of 0.2–1.5. At each point in the titration, the intermolecular PREs arising from either the specific complex or the nonspecific encounter complex ensemble were summed over their respective residues, normalized to the highest value of each titration curve, and displayed in Fig. 2.

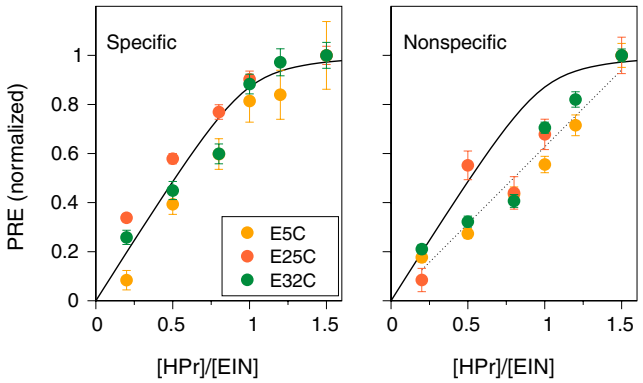

Fig. 2. Summed and normalized intermolecular PREs observed on U-[^{2}H, ^{15}N]-labeled EIN upon titration with paramagnetically labeled HPr-E5C (yellow), HPr-E25C (orange), and HPr-E32C (green). Intermolecular PRE data arising from the specific complex and nonspecific encounter complex ensemble are shown on the left and right, respectively. Data points were normalized to the highest value of each titration. A simple one-site binding curve with $K_D = 7$ μM is displayed as a black line in both panels. A linear fit to the E5C data is shown as a dotted line on the right.

For the specific PREs (Fig. 2 *Left*), the titration curves for all three paramagnetic labels saturate as the HPr concentration exceeds the EIN concentration, and the curves fit to a one-site binding isotherm using the known K_D of 7 μM (at [NaCl] = 150 mM for the specific EIN/HPr interaction determined by isothermal titration calorimetry (26) (Fig. 2 *Left*, black line). In contrast, for the nonspecific intermolecular PREs, the HPr titration curves deviate significantly from a simple one-site binding model (Fig. 2 *Right*): the curves are essentially linear and continue to increase even at equimolar concentrations of EIN and HPr, indicating the presence of a population of encounter complexes with titration behavior that is distinct from that of the specific complex.

HPr Titration Curves for Individual EIN Residues Reveal Three Types of Nonspecific Encounter Complex PREs. To characterize the different types of encounter complex configurations, we plotted the HPr titration curves (HPr-E5C, HPr-E25C, HPr-E32C) for individual residues of EIN exhibiting significant intermolecular PREs not attributable to the specific EIN/HPr complex (Fig. 1, purple circles). The PRE titration curves for the individual residues

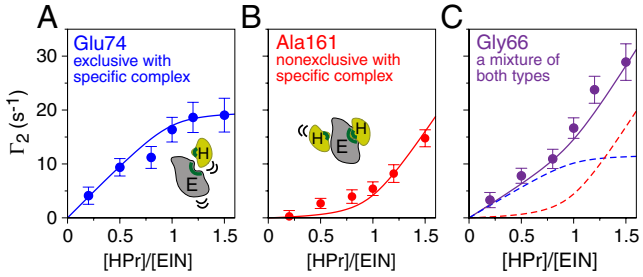

Fig. 3. Examples of HPr titration curves for the three classes of intermolecular PREs arising from the EIN/HPr encounter complex ensemble. (*A*) Class I, exemplified by the HPr-E5C titration curve for Glu74 of EIN, scales linearly with the concentration of the specific EIN/HPr complex (blue line). (*B*) Class II, exemplified by the HPr-E5C titration curve for Ala161, scales linearly with the concentration of free HPr in solution (red line). (*C*) Class III, exemplified by the HPr-E5C titration curve for Gly66, behaves as a mixture of classes I and II and fits to a scaled sum (purple line) of the specific EIN/HPr (blue dashed line) and free HPr (red dashed line) concentrations (see *Materials and Methods* for calculation details). (*Inset*) Cartoon representations of (*A*) class I and (*B*) class II encounter complex configurations of HPr (yellow) on the surface of EIN (gray), with the binding site on each protein shown in green.

partition the nonspecific PREs into three distinct classes, and examples of each type are shown in Fig. 3.

The first class of nonspecific intermolecular PREs displays the same titration behavior as the PREs arising from the specific EIN/HPr complex (Fig. 3*A*). The titration curves saturate at equimolar concentrations of EIN and HPr (Fig. 3*A*), and they fit well (reduced $\chi^2 < 1.5$ for 81% of the fits, average reduced $\chi^2 = 0.97$) to a simple single-site binding model with the K_D of 7 μM for the specific EIN/HPr interaction (Fig. 3*A*, blue line). Thus, the magnitude of the class I nonspecific PREs is directly proportional to the concentration of the specific EIN/HPr complex (Fig. 3*A*).

In contrast, the magnitude of the second class of nonspecific PREs increases only slightly at low concentrations of HPr but then rises linearly when the HPr:EIN molar ratio exceeds one (Fig. 3*B*). This titration behavior follows the concentration of unbound (i.e., free) HPr in solution, which is easily calculated from the equilibrium equation for the specific association of EIN and HPr (see *Materials and Methods*). Indeed, the HPr titration curves for the class II nonspecific PREs fit well (reduced $\chi^2 < 1.5$ for 90% of the fits, average reduced $\chi^2 = 1.1$) to calculated curves that are directly proportional to the concentration of free HPr in solution, as shown by the red line in Fig. 3*B*. (Note that the encounter complex interactions are very much weaker than the specific complex association, hence the linear dependence on the concentration of free HPr.)

The third class of nonspecific PREs behaves as a mixture of classes I and II (Fig. 3*C*). The class III titration curves follow neither a one-site binding model nor the calculated concentration of free HPr (reduced $\chi^2 \gg 1.0$). However, the titration curves do fit well to a linear combination of the two binding models with a reduced $\chi^2 < 1.5$ for 71% of the fits (average reduced $\chi^2 = 1.2$).

Fig. 4 displays the profiles of all the intermolecular PREs generated by the encounter complex configurations at the final point of the HPr titration (HPr:EIN molar ratio of 1.5). The red and blue bars indicate the relative contributions of the first and second classes of intermolecular PREs, respectively, to the total nonspecific PRE observed at a particular residue. The heteroge-

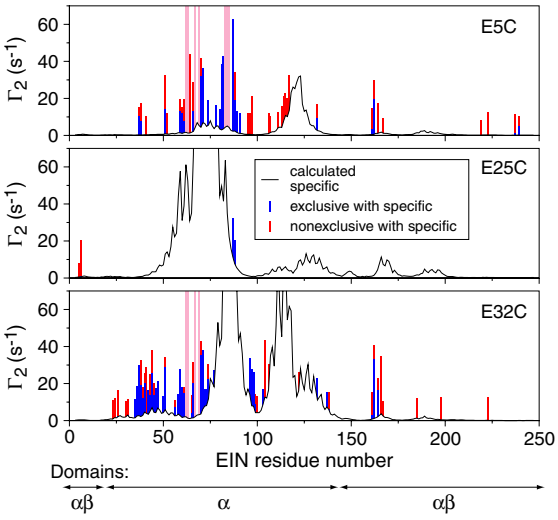

Fig. 4. Bar graphs displaying intermolecular ^1H_N-Γ_2 PRE rates observed on EIN originating from the two classes of EIN/HPr encounter complex ensembles. The data shown are for the final point of the HPr titration with 300 μM of EIN and 450 μM of HPr-E5C (*Top*), HPr-E25C (*Middle*), or HPr-E32C (*Bottom*). Relative contributions of the nonspecific PREs that scale linearly with either the concentration of the specific EIN/HPr complex (class I) or the concentration of free HPr (class II) are shown in blue and red, respectively. Intermolecular ^1H_N-Γ_2 rates back-calculated from the structure of the specific EIN/HPr complex (15) are displayed as a black line, and nonspecific PREs that are too large (>65 s^{-1}) to measure accurately are shown as pink bars.

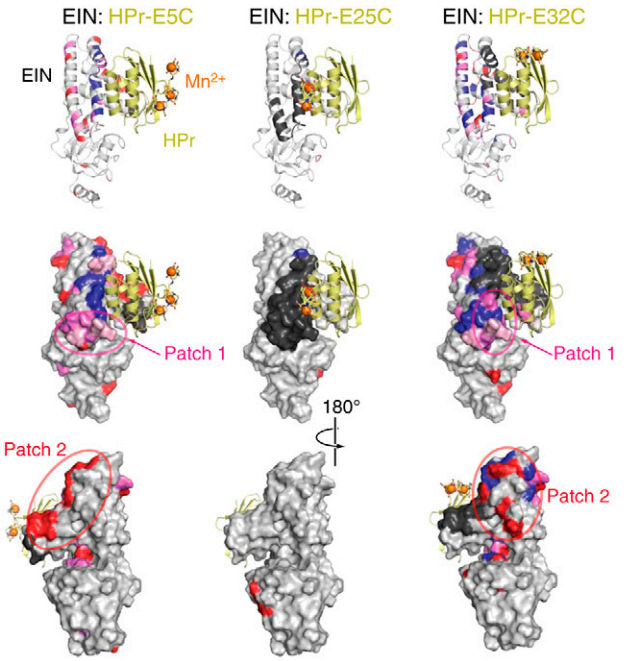

Fig. 5. Intermolecular PREs at the final titration point mapped onto the surface of EIN. Displayed as gray ribbon models in the top row and surface representations in the bottom two rows, EIN (light gray) is color coded according to the predominant (>80% contribution from classes I or II) type of intermolecular nonspecific PRE observed at a particular residue: blue, red, and purple indicate nonspecific PREs with ^1H_N-Γ_2 rates that scale linearly with the concentration of the specific EIN/HPr complex (class I), the concentration of free HPr (class II), and a mixture of both (class III), respectively. Nonspecific PREs that are too large to measure accurately ($\Gamma_2 > 65\ s^{-1}$) are in pink, and specific PREs with Γ_2 values >25 s^{-1} are in dark gray. Purple and red ellipses, labeled Patch 1 and Patch 2, respectively, highlight two regions on the surface of EIN where the class II nonspecific PREs cluster. In all three rows, HPr-E5C, HPr-E25C, and HPr-E32C (yellow ribbons) are shown in the specific configuration, and the paramagnetic EDTA-Mn^{2+} tags are displayed as a three-conformer ensemble with the Mn^{2+} atoms depicted as spheres (orange).

neity in the titration behavior of the nonspecific intermolecular PREs (Fig. 3) indicates the presence of two distinct types of interactions in the EIN/HPr encounter complex ensemble. To give physical meaning to these two encounter complex states, we mapped the intermolecular PREs for all three paramagnetic labels onto the surface of EIN (Fig. 5).

Class I Nonspecific PREs Report on Encounter Complex Interactions near the Active Site of EIN. The class I nonspecific intermolecular PREs generated by the encounter complex ensemble (Fig. 5*A*, blue) occur almost exclusively at the perimeter of the EIN active site and often coincide with specific intermolecular PREs produced by other paramagnetic probe locations (Fig. 5, dark gray). For example, HPr-E5C gives rise to nonspecific intermolecular PREs (Fig. 5 *Left*, blue) that overlap with the PREs arising from the specific EIN/HPr-E25C and EIN/HPr-E32C complexes (Fig. 5 *Center* and *Right*, dark gray).

Because the ^1H_N-Γ_2 rates for the class I nonspecific intermolecular PREs are directly proportional to the concentration of the specific EIN/HPr complex (Fig. 3*A*), these intermolecular PREs must arise from encounter complex configurations that are in equilibrium with and mutually exclusive to the specific complex (Fig. 6 *Lower Left*). Thus, the interactions that generate this first class of intermolecular PREs are unavailable once HPr occupies the active site of EIN. Given this restraint and their location on the surface of EIN (Fig. 5, blue), the first type of encounter complex states presumably involves rapid rotations and translations of HPr near or within the active site of EIN.

Rigid body rotations proximal to a high-affinity binding pocket have been predicted previously by Brownian dynamics (30) and replica exchange Monte Carlo simulations (31) on multiple protein pairs, but have been difficult to characterize experimentally because of their transient nature. These reorientations are believed to be critical for properly positioning substrate in an active site, and in the case of the EIN/HPr interaction, they probably help align the two active site histidine residues (His189 of EIN and His15 of HPr) involved in phosphotransfer from EIN to HPr. Once the proper arrangement is achieved, a network of hydrophobic interactions, hydrogen bonds, and salt bridges then lock the two proteins into the productive specific conformation (28).

Class II Nonspecific PREs Report on $HPr_{nonspecific}$/EIN/HPr Ternary Complexes. The ^1H_N-Γ_2 rates for the class II nonspecific intermolecular PREs continue to increase even at an HPr:EIN molar ratio of 1.5 (Fig. 3*B*). At this point in the titration, 96% of the EIN molecules have their active site occupied by HPr (given a $K_D = 7\ \mu M$ with EIN and HPr concentrations of 300 and 450 μM, respectively). Therefore, the class II intermolecular PREs must arise from encounter complex configurations that are *not* occluded by the specific complex but instead form a transient $HPr_{nonspecific}$/EIN/HPr ternary complex with one HPr molecule bound to the active site of EIN while another HPr molecule interacts elsewhere on the EIN surface.

The class II nonspecific intermolecular PREs cluster principally at two regions on EIN (Fig. 5, purple and red elipses, labeled "Patches"). First, both HPr-E5C (Fig. 5 *Left Middle*) and HPr-E32C (Fig. 5 *Right Middle*) give rise to strong nonspecific intermolecular PREs on the loop between α-helices 1 and 2 (centered around Phe65 and labeled as Patch 1). Second, both HPr-E5C and HPr-E32C generate a patch of nonspecific intermolecular PREs along the backside of EIN (labeled as Patch 2) at the ends of α-helices 2′ and 3 (centered at Asp95 and Ala114; Fig. 5 *Left Bottom*) and on the loop following the extended linker segment to the beginning of α-helix 1 (centered around Arg28 and Glu39; Fig. 5 *Right Bottom*), respectively.

Although the second surface patch is far from the active site of EIN, the first patch is quite close and may serve as a "docking site" for a second HPr molecule to bind while the active site of EIN is occupied and involved in phosphotransfer. This region of EIN is negatively charged with four surface glutamates, whereas the binding surface of HPr has a net positive charge (+4) with four lysines, one arginine, and one glutamate (28). Therefore, encounter complex interactions at this first cluster may accelerate specific association by properly orienting the second HPr molecule via electrostatic steering, regardless of the occupancy of the EIN active site, while also increasing the effective local concentration of HPr near the active site. In this regard it is interesting to note that recent kinetic studies and Brownian dynamics simulations on TEM1-β-lactamase and its inhibitor protein found that mutations in an encounter complex region near the specific binding site had a significantly larger effect on the overall association rate of the two proteins compared to similar types of mutations far away from the specific binding site (32).

Biological Implications of Ternary $HPr_{nonspecific}$/EIN/HPr Complexes. HPr is a master regulator of bacterial carbon metabolism that interacts not only with Enzyme I and downstream targets of the PTS system but also with many sugar transporters, transcriptional activators, antiterminators, and other regulatory kinases and phosphorylases (27). The formation of transient $HPr_{nonspecific}$/EIN/HPr ternary complexes may help Enzyme I compete for the cellular pool of HPr, even while phosphotransfer

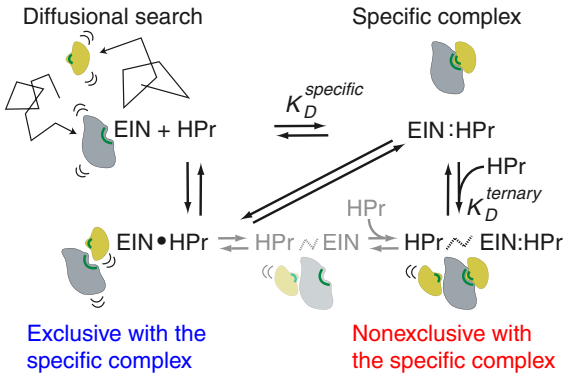

Fig. 6. Equilibrium binding model for the EIN/HPr association pathway. The intermolecular PRE data presented here indicate that, upon collision, EIN and HPr form two distinct types of weak, transient encounter complex ensembles: interactions that are in competitive equilibrium with the specific complex (*Bottom Left*), and interactions that can form simultaneously with the specific configuration to create a $HPr_{nonspecific}$/EIN/HPr ternary complex ensemble (*Bottom Right*). At the concentrations present in our experimental conditions, this second type of encounter complex rarely occurs in the absence of a specifically bound HPr and, therefore, the binary complex involving the second type of encounter complex interactions is displayed as partially transparent (*Bottom Center*).

is occurring at the EIN active site. This may be crucial to achieving high rates of sugar uptake when substrate is transiently abundant.

Indeed, conditions inside *E. coli* appear favorable for forming an $HPr_{nonspecific}$/EIN/HPr ternary complex. Given intracellular concentrations of Enzyme I and HPr of 5 and 20–100 μM, respectively (33), and a K_D of ≈10 mM for nonspecific EIN/HPr encounter complex configurations (assuming an intermolecular PRE detection limit of ≈1% for minor populated states under our experimental conditions) (14), we estimate that ≈1% of the Enzyme I molecules in vivo exist as an $HPr_{nonspecific}$/EIN/HPr ternary complex ensemble. Intracellular overcrowding and compartmentalization may favor this ternary complex further, possibly making these nonspecific interactions even more important for enhancing enzymatic turnover in vivo.

Concluding Remarks. We have presented intermolecular PRE titration experiments for the interaction of EIN and HPr that demonstrate the existence of heterogeneity in the encounter complex ensemble. Fitting a simple binding model to the intermolecular PRE data provides direct evidence for an association pathway that includes two distinct types of encounter complex configurations, as summarized in Fig. 6. The first type involves encounter complexes that are sterically occluded by the specific EIN/HPr complex (Fig. 6 *Lower Left*) and thus are probably most important for initially guiding HPr into the productive conformation when the active site is empty. The second type predominates when the active site is occupied (Fig. 6 *Lower Right*) and, therefore, is probably most important for efficiently "reloading" the EIN active site with HPr when the demand for sugar transport is high.

Materials and Methods

Sample Preparation of EIN/HPr Complexes. Uniformly labeled *E. coli* [^{2}H, ^{15}N]-EIN(1-249) and HPr at natural isotopic abundance were expressed and purified as described (29) (*SI Text*). NMR samples contained 0.3 mM U-[H^2, ^{15}N]-EIN titrated with HPr (0.06, 0.15, 0.24, 0.3, 0.36, and 0.45 mM) in 20 mM Tris-HCl, pH 7.4, and 150 mM NaCl treated with Chelex 100 (Sigma Aldrich) to remove contaminating divalent cations. HPr was paramagnetically labeled with cysteaminyl-EDTA-Mn^{2+} conjugated via a disulfide linkage to surface-engineered cysteine residues at three sites: E5C, E25C, and E32C (*SI Text*).

NMR Spectroscopy and PRE Measurements. Intermolecular transverse ^1H_N-Γ_2 PRE rates measured on the backbone amide protons of U-[^{2}H, ^{15}N]-EIN in the presence of HPr were obtained from the differences in transverse ^1H_N-R_2 relaxation rates between paramagnetic and diamagnetic samples (at identical HPr concentrations) using a transverse relaxation optimized (TROSY) version (34) of the pulse scheme depicted in figure 1 of ref. 35 (*SI Text*). Data were recorded at 40 °C on a Bruker DRX 600 MHz spectrometer equipped with a triple resonance z-gradient cryoprobe. Two time points (12 μs and 27 ms) were used for the ^1H_N-R_2 measurements, and the ^1H_N-Γ_2 rates were calculated as described (35).

Models and Data Fitting. The ^1H_N-Γ_2 rates for the encounter complex ensemble, $\Gamma_2^{EC}(\alpha)$, given by the difference between the observed intermolecular ^1H_N-Γ_2 rates and the corresponding theoretical back-calculated rates for the specific complex (see below), were fit as a function of the total HPr concentration (α) to a two-parameter model: $\Gamma_2^{EC}(\alpha) = \lambda_I c_{specific}(\alpha) + \lambda_{II} c_{free}(\alpha)$, where λ_I and λ_{II} are free parameters representing the contributions from the first and second classes of intermolecular PREs, respectively; and $c_{specific}(\alpha)$ and $c_{free}(\alpha)$ represent the concentrations of HPr bound to EIN and in free solution, respectively, calculated from the K_D of 7 μM determined by isothermal titration calorimetry (26). A standard least-squares linear regression was used to fit λ_I and λ_{II} by minimizing the appropriate χ^2:

$$\chi^2 = \sum_{\alpha} \frac{[\Gamma_2^{EC}(\alpha) - \lambda_I c_{specific}(\alpha) - \lambda_{II} c_{free}(\alpha)]^2}{\sigma_\alpha^2}$$

where σ_2 is the estimated variance in the observed intermolecular ^1H_N-Γ_2 rate at a particular EIN residue (36). To determine if a single encounter complex class could explain the intermolecular PREs as a function of HPr concentration, we first fit the data for each residue to single parameter models: $\Gamma_2^{EC}(\alpha) = \lambda_I c_{specific}(\alpha)$ or $\Gamma_2^{EC}(\alpha) = \lambda_{II} c_{free}(\alpha)$. The value of λ_I or λ_{II} obtained from these fits was used in place of the values from the two-parameter fit if the simpler model was sufficient to account for the data with a reduced $\chi^2 \leq 1.0$, if the reduced χ^2 for the single parameter fit was less than that for the two-parameter fit, or if the fitted value of either λ_I or λ_{II} from the two-parameter model was negative, indicating a nonphysical fit to the data where λ_I and λ_{II} must be ≥0.

Back-Calculation of Intermolecular PREs for the Specific Complex. The theoretical back-calculated ^1H_N-Γ_2 PRE rates for the specific complex were obtained as described (15). Briefly, experimental intramolecular ^1H_N-Γ_2 PRE rates for the three paramagnetically labeled HPr molecules were measured for the EIN/HPr complex with EIN at natural isotopic abundance and HPr isotopically labeled with ^{15}N and ^{2}H. The coordinates of the EDTA-Mn^{2+} groups, using a three-conformer ensemble representation (with atomic overlap between the EDTA groups permitted), were optimized by simulated annealing using Xplor-NIH (37) to obtain the best fit between observed and calculated intramolecular PREs for the structure of the specific EIN/HPr complex. The intramolecular PRE Q-factor (36) was 0.18, indicating excellent agreement between observed and calculated intramolecular PREs (15). The expected intermolecular PREs were then computed from the structure of the specific EIN/HPr complex (28) using the optimized coordinates of the EDTA-Mn^{2+} conformational ensembles determined from the intramolecular PREs. Further details are provided in ref. 15.

ACKNOWLEDGMENTS. We thank Gerhard Hummer for useful discussions. This work was supported by the Intramural Program of the National Institutes of Health (NIH), National Institute of Diabetes and Digestive and Kidney Diseases, and the AIDS Targeted Antiviral Program of the Office of the Director of the NIH (G.M.C.).

1. Gabdoulline RR, Wade RC (2002) Biomolecular diffusional association. *Curr Opin Struct Biol*, 12:204–213.
2. Schreiber G, Haran G, Zhou HX (2009) Fundamental aspects of protein–protein association kinetics. *Chem Rev*, 109:839–860.
3. Ubbink M (2009) The courtship of proteins: Understanding the encounter complex. *FEBS Lett*, 583:1060–1066.
4. Levy Y, Wolynes PG, Onuchic JN (2004) Protein topology determines binding mechanism. *Proc Natl Acad Sci USA*, 101:511–516.
5. Blundell TL, Fernandez-Recio J (2006) Cell biology: Brief encounters bolster contacts. *Nature*, 444:279–280.
6. Northrup SH, Boles JO, Reynolds JC (1988) Brownian dynamics of cytochrome c and cytochrome c peroxidase association. *Science*, 241:67–70.

7. Schreiber G, Fersht AR (1996) Rapid, electrostatically assisted association of proteins. *Nat Struct Mol Biol*, 3:427–431.
8. Vijayakumar M, et al. (1998) Electrostatic enhancement of diffusion-controlled protein–protein association: Comparison of theory and experiment on barnase and barstar. *J Mol Biol*, 278:1015–1024.
9. Selzer T, Albeck S, Schreiber G (2000) Rational design of faster associating and tighter binding protein complexes. *Nat Struct Mol Biol*, 7:537–541.
10. Zhou HX, Szabo A (2004) Enhancement of association rates by nonspecific binding to DNA and cell membranes. *Phys Rev Lett*, 93:178101–178104.
11. Harel M, Cohen M, Schreiber G (2007) On the dynamic nature of the transition state for protein–protein association as determined by double-mutant cycle analysis and simulation. *J Mol Biol*, 371:180–196.
12. Clore GM (2008) Visualizing lowly-populated regions of the free energy landscape of macromolecular complexes by paramagnetic relaxation enhancement. *Mol BioSyst*, 4:1058–1069.
13. Clore GM, Iwahara J (2009) Theory, practice, and applications of paramagnetic relaxation enhancement for the characterization of transient low-population states of biological macromolecules and their complexes. *Chem Rev*, 109:4108–4139.
14. Iwahara J, Clore GM (2006) Detecting transient intermediates in macromolecular binding by paramagnetic NMR. *Nature*, 440:1227–1230.
15. Tang C, Iwahara J, Clore GM (2006) Visualization of transient encounter complexes in protein–protein association. *Nature*, 444:383–386.
16. Volkov AN, Worrall JA, Holtzmann E, Ubbink M (2006) Solution structure and dynamics of the complex between cytochrome c and cytochrome c peroxidase determined by paramagnetic NMR. *Proc Natl Acad Sci USA*, 103:18945–18950.
17. Tang C, Ghirlando R, Clore GM (2008) Visualization of transient ultra-weak protein self-association in solution using paramagnetic relaxation enhancement. *J Am Chem Soc*, 130:4048–4056.
18. Tang C, Louis JM, Aniana A, Suh JY, Clore GM (2008) Visualizing transient events in amino-terminal autoprocessing of HIV-1 protease. *Nature*, 455:693–696.
19. Xu X, et al. (2008) Dynamics in a pure encounter complex of two proteins studied by solution scattering and paramagnetic NMR spectroscopy. *J Am Chem Soc*, 130:6395–6403.
20. Volkov AN, Bashir Q, Worrall JA, Ubbink M (2009) Binding hot spot in the weak protein complex of physiological redox partners yeast cytochrome c and cytochrome c peroxidase. *J Mol Biol*, 385:1003–1013.
21. Bertini I, Luchinat C, Piccioli M (2001) Paramagnetic probes in metalloproteins. *Methods Enzymol*, 339:314–340.
22. Tang C, Schwieters CD, Clore GM (2007) Open-to-closed transition in apo maltose-binding protein observed by paramagnetic NMR. *Nature*, 449:1078–1082.
23. Bertoncini CW, et al. (2005) Release of long-range tertiary interactions potentiates aggregation of natively unstructured α-synuclein. *Proc Natl Acad Sci USA*, 102:1430–1435.
24. Dedmon MM, Lindorff-Larsen K, Christodoulou J, Vendruscolo M, Dobson CM (2005) Mapping long-range interactions in alpha-synuclein using spin-label NMR and ensemble molecular dynamics simulations. *J Am Chem Soc*, 127:476–477.
25. Felitsky DJ, Lietzow MA, Dyson HJ, Wright PE (2008) Modeling transient collapsed states of an unfolded protein to provide insights into early folding events. *Proc Natl Acad Sci USA*, 105:6278–6283.
26. Suh JY, Tang C, Clore GM (2007) Role of electrostatic interactions in transient encounter complexes in protein–protein association investigated by paramagnetic relaxation enhancement. *J Am Chem Soc*, 129:12954–12955.
27. Deutscher J, Francke C, Postma PW (2006) How phosphotransferase system-related protein phosphorylation regulates carbohydrate metabolism in bacteria. *Microbiol Mol Biol Rev*, 70:939–1031.
28. Garrett DS, Seok YJ, Peterkofsky A, Gronenborn AM, Clore GM (1999) Solution structure of the 40,000 Mr phosphoryl transfer complex between the N-terminal domain of enzyme I and HPr. *Nat Struct Mol Biol*, 6:166–173.
29. Suh JY, Cai M, Clore GM (2008) Impact of phosphorylation on structure and thermodynamics of the interaction between the N-terminal domain of enzyme I and the histidine phosphocarrier protein of the bacterial phosphotransferase system. *J Biol Chem*, 283:18980–18989.
30. Spaar A, Dammer C, Gabdoulline RR, Wade RC, Helms V (2006) Diffusional encounter of barnase and barstar. *Biophys J*, 90:1913–1924.
31. Kim YC, Tang C, Clore GM, Hummer G (2008) Replica exchange simulations of transient encounter complexes in protein–protein association. *Proc Natl Acad Sci USA*, 105:12855–12860.
32. Harel M, Spaar A, Schreiber G (2009) Fruitful and futile encounters along the association reaction between proteins. *Biophys J*, 96:4237–4248.
33. Rohwer JM, Meadow ND, Roseman S, Westerhoff HV, Postma PW (2000) Understanding glucose transport by the bacterial phosphoenolpyruvate:glycose phosphotransferase system on the basis of kinetic measurements in vitro. *J Biol Chem*, 275:34909–34921.
34. Pervushin K, Riek R, Wider G, Wuthrich K (1997) Attenuated T_2 relaxation by mutual cancellation of dipole–dipole coupling and chemical shift anisotropy indicates an avenue to NMR structures of very large biological macromolecules in solution. *Proc Natl Acad Sci USA*, 94:12366–12371.
35. Iwahara J, Tang C, Clore GM (2007) Practical aspects of ^{1}H transverse paramagnetic relaxation enhancement measurements on macromolecules. *J Magn Reson*, 184:185–195.
36. Iwahara J, Schwieters CD, Clore GM (2004) Ensemble approach for NMR structure refinement against ^{1}H paramagnetic relaxation enhancement data arising from a flexible paramagnetic group attached to a macromolecule. *J Am Chem Soc*, 126:5879–5896.
37. Schwieters CD, Kuszewski J, Clore GM (2006) Using Xplor-NIH for NMR molecular structure determination. *Prog Nucl Magn Reson Spectrosc*, 48:47–62.